Experimental and Theoretical Studies of the Kinetics of the OH + Hydroxyacetone Reaction As a Function of Temperature

Munkhbayar Baasandorj,[†] Stephen Griffith, Sebastien Dusanter, and Philip S. Stevens*

Center for Research in Environmental Science, School of Public and Environmental Affairs, and Department of Chemistry, Indiana University, Bloomington, Indiana 47405

Received: May 6, 2009; Revised Manuscript Received: July 21, 2009

The rate constant for the reaction of the OH radical with hydroxyacetone was measured between 2 and 5 Torr and over the temperature range of 280−350 K, using a discharge-flow system coupled with resonance fluorescence detection of the OH radical. At 298 K the rate constant was found to be $(3.02 \pm 0.28) \times 10^{-12}$ cm^3 $molecule^{-1}$ s^{-1}, in excellent agreement with several previous studies. A positive temperature dependence was measured over the temperature range 280−350 K, described by the Arrhenius expression $k = (1.88 \pm 0.75) \times 10^{-11} \exp[-(545 \pm 60)/T]$ cm^3 $molecule^{-1}$ s^{-1}, in contrast to previous measurements of the temperature dependence for this reaction and suggesting that the atmospheric lifetime of hydroxyacetone may be greater than previously estimated. Theoretical calculations of the potential energy surface for this reaction suggest that the mechanism for this reaction involves hydrogen abstraction through a hydrogen-bonded prereactive complex similar to the OH + acetone reaction, with a calculated barrier height between −1 and 1 kcal mol^{-1} depending on the level of theory.

Introduction

Hydroxyacetone is produced in the atmosphere from the OH-initiated oxidation of methacrolein with an estimated yield of 43−47%.[1,2] Methacrolein is a major product of both the OH and the O_3-initiated oxidation of isoprene, the dominant biogenic hydrocarbon emitted by deciduous trees and various other types of vegetation.[3−5] Atmospheric concentrations of hydroxyacetone measured during the BERLOIZ campaign in Germany were highly correlated with concentrations of methacrolein and with the photochemical age of the air mass, suggesting that the primary source of hydroxyacetone is the photochemical oxidation of isoprene.[6] In addition, recent measurements of isoprene and 2-methyl-3-buten-2-ol, as well as their first-, second-, and third-generation photooxidation products above a ponderosa pine plantation found that the diurnal cycles of the second generation isoprene oxidation products (hydroxyacetone, glycolaldehyde, and methylglyoxal) were similar to their precursors.[7] However, mixing ratios of hydroxyacetone and glycolaldehyde exceeded the mixing ratios of their precursors on days with high CO and were correlated more strongly with CO than with their biogenic precursors, suggesting that anthropogenic sources of hydroxyacetone were also important.[7]

Given the abundance of isoprene throughout the troposphere, an accurate knowledge of the chemistry of hydroxyacetone is required in order to fully assess its contribution and the contribution of isoprene oxidation to the chemistry of the troposphere. In the atmosphere, reaction with OH is thought to dominate the loss of hydroxyacetone, with photolysis of only minor importance:[8]

$$OH + CH_3C(O)CH_2OH \rightarrow CH_3C(O)CHOH + H_2O \quad (1a)$$

$$OH + CH_3C(O)CH_2OH \rightarrow CH_2C(O)CH_2OH + H_2O \quad (1b)$$

$$OH + CH_3C(O)CH_2OH \rightarrow CH_3C(O)CH_2O + H_2O \quad (1c)$$

The reaction of hydroxyacetone with the OH radical is thought to proceed mainly by abstraction of a secondary H-atom (reaction 1a). The main radical product $CH_3C(O)CHOH$ reacts with O_2 rapidly in the atmosphere leading to the formation of HO_2 and methylglyoxal, which can be an important photolytic source of HO_x:[9,10]

$$CH_3C(O)CHOH + O_2 \rightarrow CH_3C(O)CHO + HO_2 \quad (2a)$$

Butkovskaya et al. reported that the yield of methylglyoxal decreases from 82% at 298 K to 49% at 236 K while the yields of formic and acetic acids increase from about 8% to about 20%.[10] Formic and acetic acids are thought to be formed by the O_2 addition to the primary radical $CH_3C(O)CHOH$ followed by decomposition of the peroxy radical:

$$CH_3C(O)CHOH + O_2 \rightarrow [CH_3C(O)CH(OH)OO] \quad (2b)$$

* To whom correspondence should be addressed. E-mail: pstevens@indiana.edu.

[†] Present address: NOAA Earth System Research Laboratory, 325 Broadway, Boulder, CO 80305.

10.1021/jp904238w CCC: $40.75
Published on Web 09/03/2009

$$[CH_3C(O)CH(OH)OO] \rightarrow HCOOH + \text{products} \quad (3a)$$

$$[CH_3C(O)CH(OH)OO] \rightarrow CH_3COOH + \text{products} \quad (3b)$$

There have been relatively few measurements of the rate constant for the reaction of hydroxyacetone with the OH radical. Dillon et al. recently measured the rate constant at 60 Torr over the temperature range 233−363 K and observed that the rate coefficient displayed a negative temperature dependence.[11] They reported a rate constant of $(5.95 \pm 0.50) \times 10^{-12}$ cm^3 molecule^{-1} s^{-1} at room temperature that is approximately a factor of 2 larger than previous measurements.[8,10,12,13]

This paper presents measurements of the rate constant for the OH + $CH_3C(O)CH_2OH$ reaction at 2 and 5 Torr and over the temperature range of 280− 350 K, using a discharge-flow system coupled with resonance fluorescence detection of the OH radical. Theoretical calculations of the potential energy surface for this reaction at various levels of theory are also presented to provide some additional insights into the energetics of this reaction.

Experimental Methods

The discharge flow system used in this study is similar to those described in detail elsewhere.[14] A schematic of the system is shown in Figure 1. The main body of the flow system consists of a 100 cm long, 2.5 cm i.d. Pyrex tube connected to an aluminum detection cell. All surfaces exposed to radicals were coated with halocarbon wax (Halocarbon Corporation) to reduce heterogeneous loss of OH radicals. Helium (Indiana Oxygen 99.995%) was added as the main carrier gas through a MKS 1179 flow controller to provide an average flow velocity of 10 m s^{-1}. A mechanical pump (Leybold D16B) downstream of the detection zone was used to evacuate the flow system. The temperature in the reaction zone was regulated by circulating heated silicon oil or cooled ethanol through the outer jacket of the flow tube, and the reaction temperature was measured by using a thermocouple inserted into the reaction zone. Pressure was measured in the middle of the reaction zone with an MKS Baratron capacitance manometer.

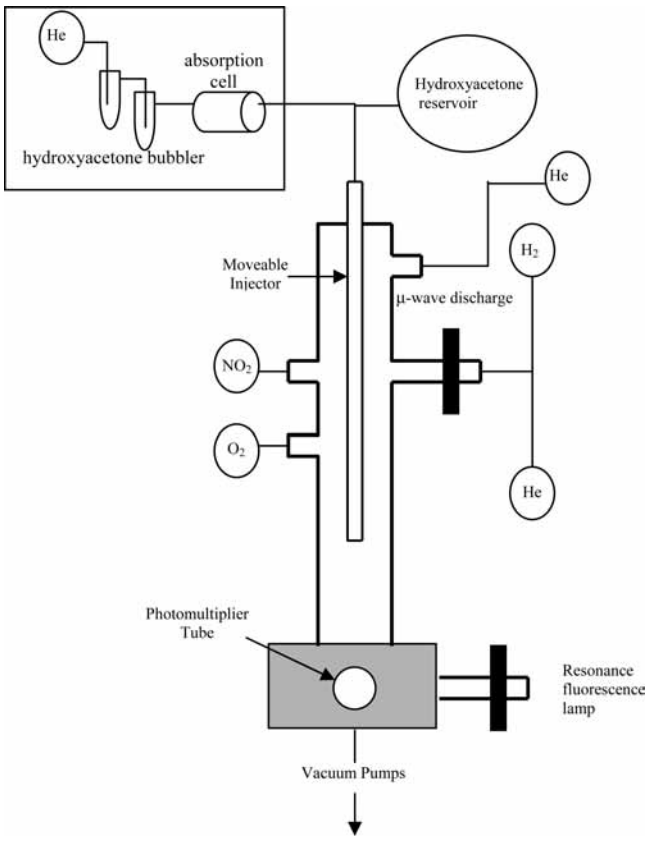

Figure 1. Schematic diagram of the discharge-flow system, showing both the reservoir system and the UV absorption system for measuring the concentration of hydroxyacetone in the flow system (see text).

OH radicals were produced by the H + $NO_2 \rightarrow$ OH + NO reaction. Hydrogen atoms were generated by a microwave discharge of H_2 (99.999% Indiana Oxygen) in the presence of helium. Excess concentrations of NO_2 (approximately 6×10^{13} cm^{-3}) were injected into the flow tube 2 cm downstream of the H atom source. OH radicals were detected by resonance fluorescence using the $A^2\Sigma^+(v'=0) \rightarrow X^2\Pi$ ($v''=0$) transition near 308 nm. The excitation radiation was produced by a microwave discharge of water vapor in the presence of helium. The OH A-X fluorescence near 308 nm was detected by a photomultiplier tube (Hamamatsu H 6180-01) located perpendicular to the radiation source. A 10 nm band-pass, 20% transmissive interference filter (Esco products) centered at 308 nm was placed in front of the photomultiplier tube to isolate the fluorescence. The OH detection sensitivity was approximately 1×10^{-8} counts s^{-1} cm^3 molecule^{-1} with a background signal of 200−300 counts s^{-1} resulting in a minimum detectable OH concentration of approximately 1×10^9 molecules cm^{-3} ($S/N = 1$, 10-s integration).

Heterogeneous loss of OH onto the reactor wall was occasionally observed with addition of hydroxyacetone to the reactor, as some experimental pseudo-first-order decays of OH were nonlinear, leading in lower than expected signals of OH as the reaction time was increased and resulting in large positive intercepts (greater than 10 s^{-1}) on the second order plots. The loss is thought to occur when OH undergoes heterogeneous reaction with hydroxyacetone adsorbed to the walls of the reactor. This behavior has been observed previously in the OH + acetone and the OH + acetic acid reactions.[15,16] The addition of oxygen (approximately $(2-5) \times 10^{15}$ cm^{-3}) or careful conditioning of the walls of the reactor with OH radicals minimized the hydroxyacetone-catalyzed loss of OH on the wall of the reactor, resulting in linear and reproducible first-order decays and intercepts in the second-order plots of less than 10 s^{-1}. The addition of oxygen to the flow reactor appears to inhibit the heterogeneous loss of hydroxyacetone on the wall of the flow reactor, but did not affect the measured second-order rate constant, as measurements made with added oxygen were consistent with measurements without added oxygen.[15,16]

Hydroxyacetone (Aldrich, > 95%; Fluka >95%) was pumped on for 2−4 h to remove water and other volatile impurities, and additionally purified by using several freeze−pump−thaw cycles. Two different methods were used for determining the concentration of hydroxyacetone in the flow reactor. In the first method, dilute mixtures of hydroxyacetone in helium were manometrically prepared by distillation of the purified mixture into a calibrated 5.5 L evacuated reservoir and diluting it with helium to a pressure of approximately 770 Torr. Mixtures with hydroxyacetone fractions of 0.4−0.6% were flowed into the reactor through a movable injector (3 mm o.d.) coated with halocarbon wax, and the concentration of the hydroxyacetone was determined by measuring the pressure drop in the calibrated reservoir over time.

The second method for determining the hydroxyacetone concentration in the reactor used UV absorption at 254 nm.[8] Helium was bubbled through a trap containing the purified sample of hydroxyacetone and injected into the system immediately after passing through a 10 cm long absorption cell. Helium flows of 40 sccm were used to maintain a pressure of 250 Torr in the absorption cell. Radiation from a low-pressure mercury lamp (11SC-1, UVP) was directed through the absorption cell and measured by a photodiode (UDT-555UV, OSI Optoelectronics). The mercury lamp and the housing in which it was enclosed were continuously purged with N_2 for temperature stabilization. A 254 nm interference filter (fwhm = 20, Acton Research Corporation) was placed directly in front of the detector, and an absorption cross section of $(5.54 \pm 0.1) \times 10^{-20}$ cm^2 molecule^{-1} at 254 nm as reported by Orlando et al.[8] was used to calculate the concentration of hydroxyacetone flowing into the reactor.

Pseudo-first-order conditions were maintained during all experiments. The OH concentrations were kept below 3×10^{11} cm^{-3} while the concentration of hydroxyacetone was varied between 3×10^{12} and 24×10^{12} cm^{-3}. Unfortunately decomposition of hydroxyacetone at higher temperatures and heterogeneous loss of OH radicals onto the reactor walls below room temperature did not allow measurements to be made above 350 K or below 280 K. Klotz et al. measured hydroxyacetone in ambient air by a wet chemical technique and noted that hydroxyacetone was found to disappear completely when subjected to a temperature of 100 °C for only a few seconds.[17]

Computational Methods

Geometry optimizations for the OH + hydroxyacetone reaction system were performed with the Gaussian 03 series of programs[18] on the Indiana University IBM Power4/Power PC970 AIX Libra cluster system. Geometries for the reactants, hydrogen-bonded adduct, and hydrogen abstraction transition state were optimized by using Becke's three-parameter hybrid method employing the LYP correction functional (B3LYP) in conjunction with 6-31G(d,p) and 6-311++G(2d,2p) basis sets, and by using second-order Møller−Plesset perturbation theory (MP2) in conjunction with the 6-31G(d,p) and 6-311++G(2d,2p) basis sets. Frequencies for all species were also calculated at each level of theory. Single point energy calculations on both the B3LYP/6-311++G(2d,2p) and MP2/6-311++G(2d,2p) optimized geometries were also done by using fourth-order Møller−Plesset perturbation theory with single, double, triple, and quadruple excitations (MP4(SDTQ)), using the 6-311++G(2d,2p) basis set.

Experimental Results

Figure 2 shows a series of pseudo-first-order decay plots for the OH + $CH_3C(O)CH_2OH$ reaction in the presence of varying concentrations of hydroxyacetone. The pseudo-first-order rate constant for a given hydroxyacetone concentration was calculated from a weighted fit (based on the precision of each measurement) of the slope of the logarithm of the OH fluorescence signal versus reaction distance, and corrected for axial diffusion and OH radical loss on the injector under the plug-flow approximation:[19]

$$k^1 = k^1_{\text{decay}}\left(1 + \frac{k^1_{\text{decay}}D}{v^2}\right) - k_{\text{injector}} \qquad \text{(I)}$$

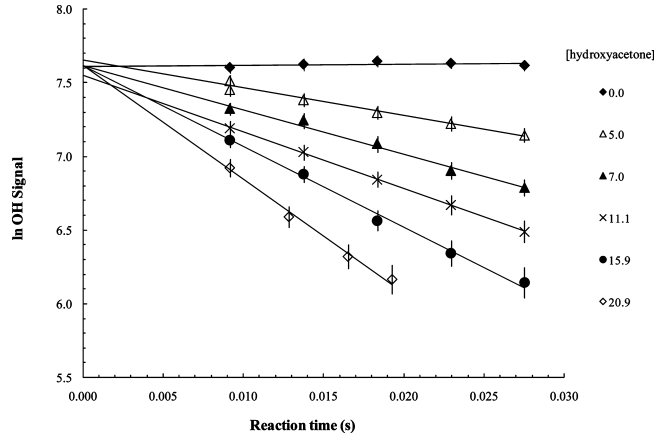

Figure 2. Pseudo-first-order decays of OH for the OH + hydroxyacetone reaction at 298 K and 5 Torr. The hydroxyacetone concentrations are in units of 10^{12} molecules cm^{-3}.

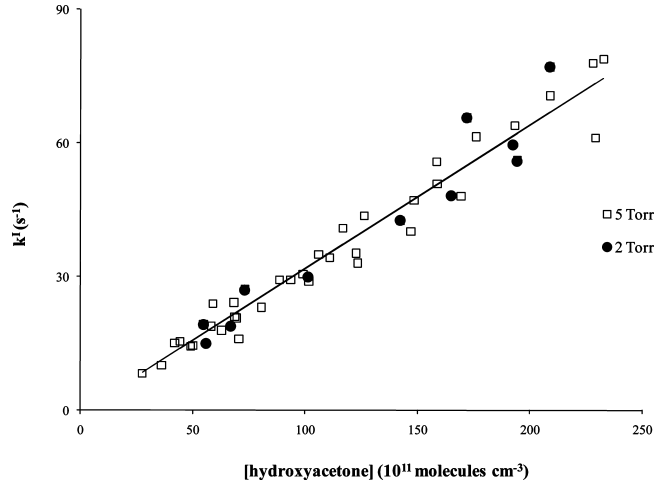

Figure 3. Second-order plots for the OH + hydroxyacetone reaction at 298 K and 2 and 5 Torr. The solid line is a weighted least-squares fit to the data (see text).

Here D is the OH diffusion coefficient in He ($0.145T^{2/3}/P_{\text{Torr}}$ cm^2 s^{-1}), v is the average flow velocity (9−14.0 m s^{-1}), and k_{injector} is the loss rate of OH on the movable injector (<10 s^{-1}), which was measured in the absence of the reagent. Figure 3 shows typical plots of the pseudo first order rates versus hydroxyacetone concentration at 298 K and 2 and 5 Torr. Corrections for axial diffusion were generally less than 5%. Second-order rate constants were obtained from a weighted least-squares fit of the measurements at each temperature. Table 1 shows the measured values at each temperature, with quoted errors of twice the standard deviation from the weighted fit.

The rate constant for the OH + hydroxyacetone reaction at 298 K and 5 Torr, using prepared reservoir mixtures of hydroxyacetone, was found to be $(3.02 \pm 0.28) \times 10^{-12}$ cm^3 molecule^{-1} s^{-1}, in excellent agreement with the room temperature values reported by Dagaut et al.,[13] Orlando et al.,[8] Chowdhury et al.,[12] and Butkovskaya et al.[10] However, it is a factor of 2 lower than the room temperature rate coefficient of $(5.95 \pm 0.50) \times 10^{-12}$ cm^3 molecule^{-1} s^{-1} reported by Dillon et al.[11] Dagaut et al.[13] determined the absolute rate constant of the reaction of hydroxyacetone with OH at 298 K using a flash photolysis resonance fluorescence technique and obtained a rate constant of $(3.0 \pm 0.3) \times 10^{-12}$ cm^3 molecule^{-1} s^{-1}. In a relative rate study, Orlando et al.[8] measured a value of $(3.0 \pm 0.7) \times 10^{-12}$ cm^3 molecule^{-1} s^{-1} at 298 K and 1 atm using methanol

TABLE 1: Summary of Experimental Results for the OH + Hydroxyacetone Reaction

T (K)	[hydroxyacetone] (10^{12} molecules cm^{-3})	k^{II} (10^{-12} cm^3 molecule^{-1} s^{-1})	pressure (Torr)
	reservoir system		
280	4.61−25.2	2.72 ± 0.48	5
288	6.60−18.8	2.98 ± 0.50	5
	5.40−20.7	2.99 ± 0.36	3
298	2.70−23.3	3.02 ± 0.28	5
	5.59−21.2	2.81 ± 0.38	2
317	4.83−24.4	3.54 ± 0.42	5
322	5.35−21.1	3.31 ± 0.41	5
334	4.94−13.7	3.81 ± 0.70	5
342	2.00−19.2	3.99 ± 0.34	5
	5.70−20.0	3.80 ± 0.62	2
347	5.10−22.2	3.93 ± 0.52	5
	absorption cell (254 nm)		
318	2.79−41.1	3.11 ± 0.39	5
350	4.09−26.2	3.83 ± 0.54	5

and ethanol as reference compounds. The loss of hydroxyacetone and the reference compounds were quantified by using FTIR spectroscopy. Chowdhury et al.[12] reported a value of (2.8 ± 0.2) × 10^{-12} cm^3 molecule^{-1} s^{-1} using laser photolysis with laser-induced fluorescence detection of OH radicals. Butkovskaya et al.[10] reported a value of (3.17 ± 0.22) × 10^{-12} cm^3 molecule^{-1} s^{-1} for the OH + hydroxyacetone reaction at 298 K using a turbulent flow reactor at 200 Torr and detection of OH by chemical ionization mass spectrometry. Butkovskaya et al. also measured the rate constant for the OD + hydroxyacetone reaction, reporting a value of (4.08 ± 0.31) × 10^{-12} cm^3 molecule^{-1} s^{-1}, resulting in a secondary kinetic isotope effect of 0.78 ± 0.10, similar to that observed for the OH + acetone reaction.[20] Dillon et al.[11] used a pulsed photolysis laser-induced fluorescence technique to determine the rate constant for the OH + hydroxyacetone reaction over the temperature range 233−363 K at 60 Torr. Concentrations of hydroxyacetone were determined by UV absorption at 184.9 nm downstream of the reactor, using a measured cross section of $\sigma_{184.9nm}$ = (5.43 ± 0.08) × 10^{-18} cm^2 molecule^{-1}.

The measurements of the rate coefficients for the OH + hydroxyacetone reaction as a function of temperature are shown in Figure 4. In this figure, the rate constants measured in this study using the reservoir system to determine the hydroxyacetone concentration are shown as the solid red circles, and exhibit a positive temperature dependence. A weighted least-squares fit of the data as a function of temperature yields the following Arrhenius expression for the rate constant between 280 and 350 K and 2−5 Torr:

$$k = (1.88 \pm 0.75) \times 10^{-11} \exp\left(-\frac{545 \pm 60}{T}\right) \text{cm}^3 \text{ molecule}^{-1} \text{ s}^{-1} \quad \text{(II)}$$

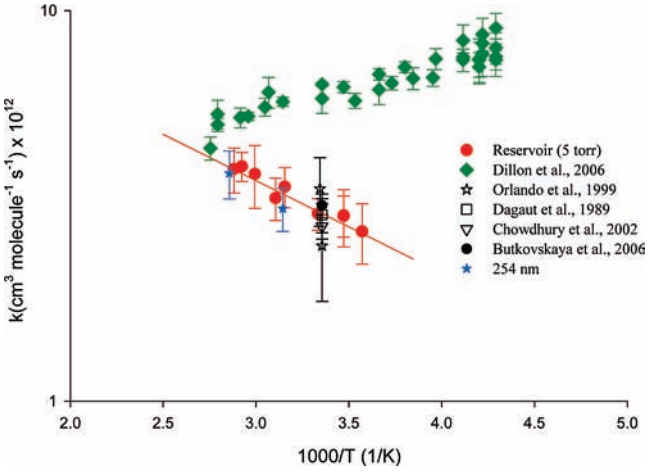

Figure 4. Arrhenius plot for the OH + hydroxyacetone reaction. The data from this work include measurements where the hydroxyacetone concentration was determined from the flow from a calibrated reservoir, as well as measurements where the hydroxyacetone concentrations were determined by using absorption at 254 nm (see text). The solid line is a fit to the data reported here.

The measurements of the rate constant for this reaction by using UV absorption at 254 nm with the absorption cross section reported by Orlando et al.[8] (solid blue stars in Figure 3) at 318 K and 350K are in good agreement with those obtained in this study by using the reservoir system. These results are in contrast to the results of Dillon et al., who reported a negative temperature dependence at 60 Torr described by the expression k = (2.15 ± 0.30) × 10^{-12} exp[(305 ± 10)/T] cm^3 molecule^{-1} s^{-1}.[11]

Discussion

The source of the discrepancy between the measurements reported by Dillon et al. with the measurements reported here is unclear. One possible source of error in the measurements reported here is the uncertainty associated with the determination of the concentration of hydroxyacetone in the reactor and its potential loss on surfaces.[11] However, the agreement of the measurements reported here by using two different methods for introducing and measuring the concentration of hydroxyacetone into the reactor with different residence times, concentrations, and surface areas suggests that loss of hydroxyacetone on the glass walls of the reservoir or the absorption cell is not significantly affecting the measured rate constants. Unfortunately, the concentration of hydroxyacetone cannot be measured at the exit of our experimental system. However, the linearity of the pseudo-first-order decays also suggests that significant loss of hydroxyacetone on the walls of the reactor, which would increase as the reaction distance increases since hydroxyacetone is added through the movable injector, is not affecting the measured rate constants.

As discussed by Dillon et al., one possible explanation for the factor of 2 difference between their measurements near room temperature and the previous measurements is an error in the measured absorption cross section of hydroxyacetone at 184.9 nm used to calculate the concentration of hydroxyacetone in their experiments. However, Dillon et al. report measurements of the absorption cross section at 254 nm relative to their measurements at 184.9 nm that were in excellent agreement with the value reported by Orlando et al.[8,11] We performed similar measurements at room temperature by setting up a constant flow of hydroxyacetone through the absorption cell described above and measured the absorption at 185 nm relative to 254 nm by exchanging the 254 nm bandpass filter with one centered at 185 nm (Acton Research Corporation). Measurements of the transmission of radiation at 254 nm through the 185 nm filter were made by using a flow of nitrogen containing 26% nitrous oxide that absorbs more than 99% of the photons at 184.9 nm and less than 0.1% at 253.7 nm. After correcting for the transmission of 254 nm radiation, measurements of the absorption at 185 nm were approximately a factor of (80 ± 10) times greater than that at 254 nm, which is within 20% of the ratio of the absolute cross section measurement of Dillon et al. at 184.9 nm ($\sigma_{184.9nm}$ = (5.43 ± 0.08) × 10^{-18} cm^2 molecule^{-1})

TABLE 2: Energies, Zero-Point Energies (hartrees), and Zero Point Corrected Relative Energies (kcal/mol) for Hydrogen Abstraction in the OH + Hydroxyacetone Reaction

	B3LYP/6-311++G(2d,2p)				MP4/6-311++G(2d,2p)// B3LYP/6-311++G(2d,2p)			
	energy	ZPE	S^2	E_{rel}	energy	ZPE	S^2	E_{rel}
OH	−75.76432	0.00848	0.752		−75.61413	0.00848	0.757	
HAC	−268.46853	0.08900	0		−267.86612	0.08900	0	
COM	−344.24205	0.10031	0.752	−4.0	−343.49089	0.10031	0.756	−4.9
TS	−344.23829	0.09888	0.754	−2.5	−343.48321	0.09888	0.759	−1.0
	MP2/6-311++G(2d,2p)				MP4/6-311++G(2d,2p)// MP2/6-311++G(2d,2p)			
	energy	ZPE	S^2	E_{rel}	energy	ZPE	S^2	E_{rel}
OH	−75.59737	0.00871	0.757		−75.61413	0.00871	0.757	
HAC	−267.79622	0.09022	0		−267.86635	0.09022	0	
COM	−343.40451	0.10192	0.756	−5.0	−343.49136	0.10192	0.756	−4.9
TS	−343.38799	0.09702	0.778	2.3	−343.47640	0.09702	0.778	1.3

relative to that measured by Orlando et al. at 254 nm ($\sigma_{254nm} = (5.54 \pm 0.1) \times 10^{-20}$ cm^2 molecule^{-1}).[8,11] As a result, it appears unlikely that an error in the measured absorption cross section at 184.9 nm can account for the factor of 2 difference in the reported rate constant at 298 K between the measurements of Dillon et al. and the results reported here and the previous measurements described above.

Other potential sources of error discussed by Dillon et al. include reactive impurities or photolysis products of hydroxyacetone, such as formaldehyde, that could enhance the observed rate and affect the observed temperature dependence, although it appears that these interferences have been minimized through the use of purified samples and low laser fluences.[11] However, Dillon et al. estimated that it would only take a 10−20% aldehyde impurity to account for a factor of 2 increase in the rate constant.[11] Dillon et al. did observe nonexponential behavior in their pseudo-first-order decays of OH at longer reaction times, which they attributed to secondary production of OH from the alkyl radical products of the reaction, or from H atoms produced from the 248 nm O_3-CH_4 photolytic OH source leading to OH formation from the $H + O_3 \rightarrow OH + O_2$ reaction.[11]

Recycling of OH radicals at long reaction times could lead to an underestimation of the overall rate constant for the OH + hydroxyacetone reaction. In the presence of O_2, Butkovskaya et al. observed the production of OH radicals from the OD + hydroxyacetone reaction, resulting in a reported yield of approximately 10% at 298 K.[10] This formation of OH radicals may be the result of the addition reaction of the $CH_3C(O)CHOH$ radical product with O_2 and subsequent decomposition of the resulting peroxy radical to form OH and either formic or acetic acid (reactions 3a and 3b). The observed OH yield was consistent with the observed acid yield.[10] Similar measurements of the OH yield from the OD + hydroxyacetone reaction as part of this study were unsuccessful due to high concentrations of OH radicals produced from water impurities in the microwave discharge. The small production of OH from this mechanism would lead to slower observed pseudo-first-order decays and a slower observed rate constant for the OH + hydroxyacetone reaction. However, kinetic simulations suggest that under the conditions of the experiments reported here the production of OH by this mechanism would reduce the observed rate constant by approximately 10% over the temperature range studied, which is within the error of these measurements. In addition, the agreement of the rate constant measured with and without added oxygen also suggests that this OH recycling mechanism is not significantly interfering with the measured rate constant, as the production of OH by reactions 3a and 3b should be slower under low concentrations of O_2.[10] As a result, the source of the discrepancy between the measurements reported by Dillon et al. with the measurements reported here is unclear.

There have been several theoretical studies of the mechanism for the OH + hydroxyacetone reaction. A detailed ab initio study by Gallano found several hydrogen-bonded prereactive complexes corresponding to each product channel, with stabilization energies ranging from −3.4 to −4.8 kcal/mol relative to the reactants at the CCSD(T)//BHandHLYP/ 6-311++G(d,p) level of theory, with the most stable complex corresponding to reaction 1a.[21] Gallano also found transition states energies corresponding to each channel ranging from −1.1 to 4.4 kcal/mol, with the lowest energy transition state corresponding to hydrogen abstraction from the methylene group (reaction 1a).[21] Dillon et al. found stabilization energies for the prereactive complexes ranging from −1.6 to −5.7 kcal/mol relative to reactants at the CCSD(T)//B3LYP/6-311(d,p) level of theory, and transition state energies for each channel ranging from 3 to 5 kcal/mol relative to reactants with the lowest transition state energy corresponding to reaction 1a.[11] These theoretical results are consistent with the product studies by Butkovskaya et al.[10] that suggest that the reaction proceeds mainly by hydrogen abstraction from the methylene (CH_2OH) group (reaction 1a).

To provide additional insight into the potential energy surface for this reaction, the structures of the reactants, hydrogen-bonded complex, and hydrogen abstraction transition state for reaction 1a were initially optimized at both the B3LYP/6-31G(d,p) and MP2/6-31G(d,p) levels of theory, and further optimized at the B3LYP/6-311++G(2d,2p) and MP2/6-311++G(2d,2p) levels of theory. Single point energy calculations at the MP4(SDTQ)/6-311++G(2d,2p) level of theory were done on both the MP2/6-311++G(2d,2p) and B3LYP/6-311++G(2d,2p) optimized geometries. For simplicity, only the hydrogen-bonded complex and transition state for hydrogen abstraction from the methylene group is considered here, as it is the most stable prereactive complex and will contribute the most to the thermal equilibrium population. The optimized transition state at each level of theory was confirmed to correspond to the prereactive complex and products by following the intrinsic reaction coordinate (IRC) in both the forward and backward directions in addition to an analysis of the vector of the imaginary frequency.

The relative energies along with the spin eigenvalues (S^2) for the reactants, prereactive complex, and the corresponding transition state at the higher levels of theory are summarized in Table 2. Contamination of the wave function from higher spin states at each level of theory is minimal, as the expected value for S^2 for each is within 5% of the exact value of 0.750 for a pure doublet. Frequencies for the reactants, stabilized complex, transition state, and products were calculated at both the B3LYP/

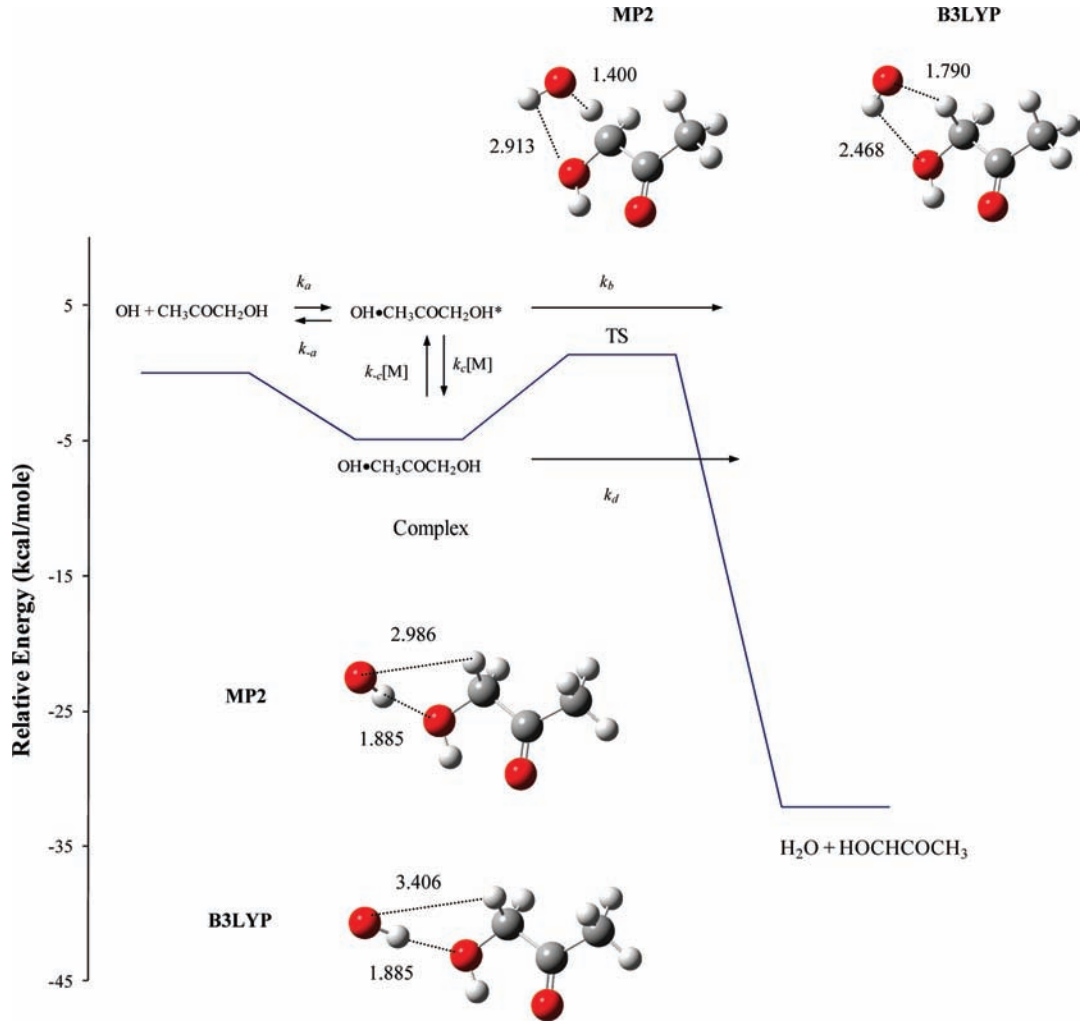

Figure 5. A schematic representation of the mechanism for the methylene H-abstraction channel for the OH + hydroxyacetone reaction. Energies are those calculated at the MP4(SDTQ)/6-311++G(2d,2p)//MP2/6-311++G(2d,2p) level of theory (see text). Both the MP2/6-311++G(2d,2p) and B3LYP/6-311++G(2d,2p) optimized geometries for the complex and transition state are shown for comparison.

6-311++G(2d,2p) and MP2/6-311++G(2d,2p) levels of theory, and these frequencies were used to calculate the zero point energy (ZPE) at the corresponding level of theory.

As can be seen from this table, the calculated stabilization energy of the prereactive complex is similar for the higher levels of theory used in this study, varying from 4.0 kcal mol^{-1} at the B3LYP/6-311++G(2d,2p) + ZPE level of theory, to 5.0 kcal mol^{-1} at the MP2/6-311++G(2d,2p) + ZPE level of theory. The optimized geometries for the prereactive complex and reactants are similar at these levels of theory, and as a result the MP4(SDTQ)/6-311++G(2d,2p) + ZPE calculated energies of the complex at the B3LYP and MP2 optimized geometries are also similar (4.9 kcal mol^{-1}). The zero-point corrected stability of the prereactive complex calculated at the MP4(SDTQ)/6-311++G(2d,2p)//MP2/6-311++G(2d,2p) level of theory (4.9 kcal mol^{-1}) is similar to the stabilization energy of 5.68 kcal mol^{-1} calculated by Dillon et al. for the same complex at the CCDSD(T)/6-311G(d,p)//B3LYP/6-311G(d,p) level of theory,[11] as well as the value of 4.6 kcal/mol^{-1} calculated by Galano for the same complex at the CCSD(T)//BHandHLYP/6-311++G(d,p) level of theory.[21] The results presented here are also comparable to the value of 4.6 kcal mol^{-1} calculated for the OH + acetone reaction at the B3LYP/6-311++G(2d,2p) level of theory.[15,22]

In contrast, the calculated energy of the transition state relative to the reactants does depend on the level of theory, ranging from −2.5 kcal mol^{-1} at the B3LYP/6-311++G(2d,2p) + ZPE level of theory to +2.3 kcal mol^{-1} at the MP2/6-311++G(2d,2p) + ZPE level of theory (Table 2). The difference in the calculated barrier height at the different levels of theory is partly due to the difference in the B3LYP and MP2 optimized geometries of the transition state (Figure 5). The B3LYP/6-311++G(2d,2p) optimized transition state corresponds to a point earlier along the reaction coordinate, as the distance between the OH oxygen and the methylene hydrogen is longer (1.790 Å) at this level of theory compared to that for the MP2/6-311++G(2d,2p) optimized geometry (1.400 Å). Calculated energies for each optimized transition state and reactants at the MP4(SDTQ)/6-311++G(2d,2p) + ZPE level of theory varied from −1.0 kcal mol^{-1} for the B3LYP/6-311++G(2d,2p) optimized transition state geometry to 1.3 kcal mol^{-1} for the MP2/6-311++G(2d,2p) optimized transition state geometry. The calculated energy of the transition state of −1 kcal mol^{-1} relative to reactants at the MP4(SDTQ)/6-311++G(2d,2p)//B3LYP/6-311++G(2d,2p) + ZPE level of theory is similar to the value of −1.1 kcal mol^{-1} calculated by Galano at the CCSD(T)//BHandHLYP/6-311++G(d,p) level of theory.[21] In contrast, the calculated energy of the transition state of +1.3 kcal mol^{-1} relative to the reactants at the MP4(SDTQ)/6-311++G(2d,2p) //MP2/6-311++G(2d,2p) level of theory is similar to the estimated barrier height of approximately +3 kcal mol^{-1} calculated by Dillon et al. at the

CCSD(T)//B3LYP/6-31G(d,p) level of theory.[11] Similar differences in calculated barrier heights at different levels of theory have been seen previously for the OH + acetone reaction. At the B3LYP/6-311++G(2d,2p) level of theory the calculated barrier height relative to reactants is −1.1 kcal mol^{-1}.[15] In contrast, the CBS-QB3//B3LYP/6-311G(d,p) transition state energies for the OH + acetone reaction of Yamada et al. determined by using the IRCmax method resulted in a barrier of approximately +2 kcal/mol, similar to the experimental activation energy.[23]

An overall barrier height and activation energy for the OH + hydroxyacetone reaction that is smaller than that for the OH + acetone reaction is not surprising as the energy of the transition state in the OH + hydroxyacetone reaction is likely lower than that for the OH + acetone reaction due to the weakening of the C−H bond in hydroxyacetone from the presence of the hydroxyl group.[11] In addition, entropic factors may also favor the OH + hydroxyacetone reaction compared to the OH + acetone reaction, as no rotational degrees of freedom are lost in the transition state for the OH + hydroxyacetone reaction resulting in a higher density of states.[11] These factors can account for the larger rate constant for the OH + hydroxyacetone reaction compared to the OH + acetone reaction.[11]

A schematic of the potential energy surface for the OH + hydroxyacetone reaction calculated at the MP4(SDTQ)/6-311++G(2d,2p)//MP2/6-311++G(2d,2p) level of theory is shown in Figure 5. These energies correspond to H abstraction from the $-CH_2OH$ group (reaction 1a) through the prereactive complex involving the attractive interaction between the H atom in the OH radical and the O atom of the hydroxyl group in hydroxyacetone. Similar to the reactions of OH with acetone, acetic acid, and nitric acid, the first step of the mechanism involves the formation of excited OH-HAC* complex which can dissociate to reform the reactants, react to form the products, or be collisionally stabilized to form the thermalized OH-HAC complex. The thermalized complex can be collisionally activated to form the excited complex or react to form products.[15,16,24−27]

It is possible that the observed difference in the temperature dependence reported here at 5 Torr for the OH + hydroxyacetone reaction with that observed by Dillon et al. at 60 Torr may be due to an unusual pressure dependence for this reaction. Brown et al. observed that the rate constant for the reaction of OH with nitric acid showed a different temperature dependence at low pressure compared to high pressure.[24,27] This unusual dependence on pressure and temperature is likely a result of a competition between the reactions of the excited complex with collisional stabilization and the reactions of the stabilized complex with collisional excitation. Additional measurements of the temperature dependence of the OH + hydroxyacetone reaction at different pressures are needed to resolve the discrepancy in the measured temperature dependence for this reaction.

The observed temperature dependence reported here is also in contrast to the calculations of Galano, who predicted a negative temperature dependence for the OH + hydroxyacetone reaction using conventional transition state theory.[21] Although the room temperature rate constant calculated in this study is in excellent agreement with the room temperature rate constant reported here, the calculated negative temperature dependence likely arises from the assumption that the energy of the lowest lying transition state is below the energy of the reactants. However, as discussed above there is a large uncertainty associated with the barrier height for the lowest lying transition state, similar to the range of predicted transition state energies for the OH + acetone and OH + acetic acid reactions.[15,16] Clearly additional theoretical calculations are needed in order to resolve these discrepancies.

Conclusions

Measurements of the rate constant for the OH + hydroxyacetone reaction at 298 K and 5 Torr are in excellent agreement with several previous studies.[8,12,13] However, the measurements reported here are a factor of 2 lower than the value at 298 K recently reported by Dillon et al.[11] A positive temperature dependence for the OH + hydroxyacetone reaction was also observed in contrast to the negative temperature dependence observed by Dillon et al.[11] The reasons for these discrepancies are unclear.

Theoretical calculations of the potential energy surface using geometries optimized at both the B3LYP/6-311++G(2d,2p) and MP2/6-311++G(2d,2p) levels of theory, with additional single point energy calculations at the MP4(SDTQ)/6-311++G(2d,2p) level of theory, suggest that the barrier for the lowest lying transition state is between −1 and 1 kcal mol^{-1}. Although this small barrier height is consistent with the temperature dependence reported here, additional measurements and theoretical studies are needed to help resolve the discrepancy in the measured temperature dependence for this reaction. The experimental results presented here suggest that the atmospheric lifetime of hydroxyacetone relative to reaction with OH may be longer than previously estimated, especially at temperatures relevant to the upper troposphere.

Acknowledgment. We would like to thank Kenta Caldwell and Elisabeth Gawthrop for experimental assistance. This work was supported the National Science Foundation (grant ATM-0622815).

Supporting Information Available: Geometries, energies and vibrational frequencies of all structures calculated in this study. This material is available free of charge via the Internet at http://pubs.acs.org.

References and Notes

(1) Tuazon, E. C.; Atkinson, R. *Int. J. Chem. Kinet.* **1990**, *22*, 591.
(2) Orlando, J. J.; Tyndall, G. S.; Paulson, S. E. *Geophys. Res. Lett.* **1999**, *26*, 2191.
(3) Tuazon, E. C.; Atkinson, R. *Int. J. Chem. Kinet.* **1990**, *22*, 1221.
(4) Paulson, S. E.; Flagan, R. C.; Seinfeld, J. H. *Int. J. Chem. Kinet.* **1992**, *24*, 79.
(5) Paulson, S. E.; Seinfeld, J. H. *J. Geophys. Res., [Atmos.]* **1992**, *97*, 20703.
(6) Grossmann, D.; Moortgat, G. K.; Kibler, M.; Schlomski, S.; Bachmann, K.; Alicke, B.; Geyer, A.; Platt, U.; Hammer, M. U.; Vogel, B.; Mihelcic, D.; Hofzumahaus, A.; Holland, F.; Volz-Thomas, A. *J. Geophys. Res., [Atmos.]* **2003**, *108*, 20.
(7) Spaulding, R. S.; Schade, G. W.; Goldstein, A. H.; Charles, M. J. *J. Geophys. Res., [Atmos.]* **2003**, *108*, 17.
(8) Orlando, J. J.; Tyndall, G. S.; Fracheboud, J. M.; Estupinan, E. G.; Haberkorn, S.; Zimmer, A. *Atmos. Environ.* **1999**, *33*, 1621.
(9) Jenkin, M. E.; Cox, R. A.; Emrich, M.; Moortgat, G. K. *J. Chem. Soc., Faraday Trans.* **1993**, *89*, 2983.
(10) Butkovskaya, N. I.; Pouvesle, N.; Kukui, A.; Mu, Y. J.; Le Bras, G. *J. Phys. Chem. A* **2006**, *110*, 6833.
(11) Dillon, T. J.; Horowitz, A.; Holscher, D.; Crowley, J. N.; Vereecken, L.; Peeters, J. *Phys. Chem. Chem. Phys.* **2006**, *8*, 236.
(12) Chowdhury, P. K.; Upadhyaya, H. P.; Naik, P. D.; Mittal, J. P. *Chem. Phys. Lett.* **2002**, *351*, 201.
(13) Dagaut, P.; Liu, R. Z.; Wallington, T. J.; Kurylo, M. J. *J. Phys. Chem.* **1989**, *93*, 7838.
(14) Stevens, P.; L'Esperance, D.; Chuong, B.; Martin, G. *Int. J. Chem. Kinet.* **1999**, *31*, 637.
(15) Davis, M. E.; Drake, W.; Vimal, D.; Stevens, P. S. *J. Photochem. Photobiol., A* **2005**, *176*, 162.

(16) Vimal, D.; Stevens, P. S. *J. Phys. Chem. A* **2006**, *110*, 11509.

(17) Klotz, P. J.; Kwok, E. S. C.; Zhou, X.; Lee, J. H.; Lee, Y. N. *A measurement technique for hydroxyacetone*; Brookhaven National Laboratory: Uptown, NY, 1999.

(18) Frisch, M. J.; Trucks, G. W.; Schlegel, H. B.; Scuseria, G. E.; Robb, M. A.; Cheeseman, J. R.; Montgomery, J. A., Jr.; Vreven, T.; Kudin, K. N.; Burant, J. C.; Millam, J. M.; Iyengar, S. S.; Tomasi, J.; Barone, V.; Mennucci, B.; Cossi, M.; Scalmani, G.; Rega, N.; Petersson, G. A.; Nakatsuji, H.; Hada, M.; Ehara, M.; Toyota, K.; Fukuda, R.; Hasegawa, J.; Ishida, M.; Nakajima, T.; Honda, Y.; Kitao, O.; Nakai, H.; Klene, M.; Li, X.; Knox, J. E.; Hratchian, H. P.; Cross, J. B.; Bakken, V.; Adamo, C.; Jaramillo, J.; Gomperts, R.; Stratmann, R. E.; Yazyev, O.; Austin, A. J.; Cammi, R.; Pomelli, C.; Ochterski, J. W.; Ayala, P. Y.; Morokuma, K.; Voth, G. A.; Salvador, P.; Dannenberg, J. J.; Zakrzewski, V. G.; Dapprich, S.; Daniels, A. D.; Strain, M. C.; Farkas, O.; Malick, D. K.; Rabuck, A. D.; Raghavachari, K.; Foresman, J. B.; Ortiz, J. V.; Cui, Q.; Baboul, A. G.; Clifford, S.; Cioslowski, J.; Stefanov, B. B.; Liu, G.; Liashenko, A.; Piskorz, P.; Komaromi, I.; Martin, R. L.; Fox, D. J.; Keith, T.; Al-Laham, M. A.; Peng, C. Y.; Nanayakkara, A.; Challacombe, M.; Gill, P. M. W.; Johnson, B.; Chen, W.; Wong, M. W.; Gonzalez, C.; Pople, J. A. *Gaussian 03*, Revision B.05; Gaussian, Inc., Wallingford, CT, 2004.

(19) Howard, C. J. *J. Phys. Chem.* **1979**, *83*, 3.

(20) Gierczak, T.; Gilles, M. K.; Bauerle, S.; Ravishankara, A. R. *J. Phys. Chem. A* **2003**, *107*, 5014.

(21) Galano, A. *J. Phys. Chem. A* **2006**, *110*, 9153.

(22) Aloisio, S.; Francisco, J. S. *J. Phys. Chem. A* **2000**, *104*, 3211.

(23) Yamada, T.; Taylor, P. H.; Goumri, A.; Marshall, P. *J. Chem. Phys.* **2003**, *119*, 10600.

(24) Brown, S. S.; Talukdar, R. K.; Ravishankara, A. R. *J. Phys. Chem. A* **1999**, *103*, 3031.

(25) Smith, I. W. M.; Ravishankara, A. R. *J. Phys. Chem. A* **2002**, *106*, 4798.

(26) Talukdar, R. K.; Gierczak, T.; McCabe, D. C.; Ravishankara, A. R. *J. Phys. Chem. A* **2003**, *107*, 5021.

(27) Brown, S. S.; Burkholder, J. B.; Talukdar, R. K.; Ravishankara, A. R. *J. Phys. Chem. A* **2001**, *105*, 1605.

JP904238W